Cell Reports

Resource

Systematic Genetic Screens Reveal the Dynamic Global Functional Organization of the Bacterial Translation Machinery

Graphical Abstract

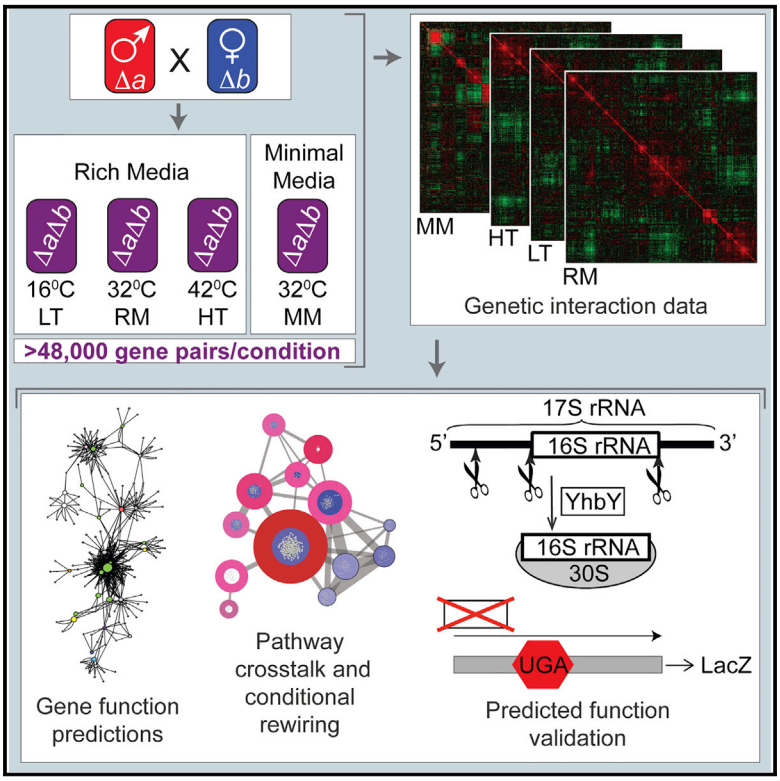

Highlights

- Conditional genetic interaction maps underlying microbial protein synthesis
- Identification of functionally associated genes, pathways, and adaptive responses
- Striking protein synthesis defects upon the loss of identified unannotated genes
- Links among connectivity, conditional rewiring, and evolutionary adaptation

Authors

Alla Gagarinova, Geordie Stewart, Bahram Samanfar, ..., Eric D. Brown, Mohan Babu, Andrew Emili

Correspondence

andrew.emili@utoronto.ca

In Brief

Gagarinova et al. used *Escherichia coli* synthetic genetic arrays to map genetic interactions underlying protein synthesis. The data revealed functionally overlapping genes, pathways, and adaptive responses, as well as the functions of previously uncharacterized genes required for normal translation. The results have implications for evolutionary studies of biological systems.

Gagarinova et al., 2016, Cell Reports *17*, 904–916
October 11, 2016
http://dx.doi.org/10.1016/j.celrep.2016.09.040

CellPress

OPEN ACCESS
CellPress

Cell Reports
Resource

Systematic Genetic Screens Reveal the Dynamic Global Functional Organization of the Bacterial Translation Machinery

Alla Gagarinova,[1,2] Geordie Stewart,[3] Bahram Samanfar,[4,5] Sadhna Phanse,[2,6] Carl A. White,[2] Hiroyuki Aoki,[6] Viktor Deineko,[6] Natalia Beloglazova,[7] Alexander F. Yakunin,[7] Ashkan Golshani,[4] Eric D. Brown,[3] Mohan Babu,[2,5] and Andrew Emili[1,2,8,*]

[1]Department of Molecular Genetics, University of Toronto, Toronto, ON M5S 1A8, Canada
[2]Donnelly Centre for Cellular and Biomolecular Research, University of Toronto, Toronto, ON M5S 3E1, Canada
[3]Department of Biochemistry and Biomedical Sciences, M.G. DeGroote Institute for Infectious Disease Research, McMaster University, Hamilton, ON L8N 3Z5, Canada
[4]Department of Biology and the Ottawa Institute of Systems Biology, Carleton University, Ottawa, ON K1S 5B6, Canada
[5]Agriculture and Agri-Food Canada, Ottawa Research and Development Centre, Ottawa, ON K1A 0C6, Canada
[6]Department of Biochemistry, Research and Innovation Centre, University of Regina, Regina, SK S4S 0A2, Canada
[7]Department of Chemical Engineering and Applied Chemistry, University of Toronto, Toronto, ON M5S 3E5, Canada
[8]Lead Contact
*Correspondence: andrew.emili@utoronto.ca
http://dx.doi.org/10.1016/j.celrep.2016.09.040

SUMMARY

Bacterial protein synthesis is an essential, conserved, and environmentally responsive process. Yet, many of its components and dependencies remain unidentified. To address this gap, we used quantitative synthetic genetic arrays to map functional relationships among >48,000 gene pairs in *Escherichia coli* under four culture conditions differing in temperature and nutrient availability. The resulting data provide global functional insights into the roles and associations of genes, pathways, and processes important for efficient translation, growth, and environmental adaptation. We predict and independently verify the requirement of unannotated genes for normal translation, including a previously unappreciated role of YhbY in 30S biogenesis. Dynamic changes in the patterns of genetic dependencies across the four growth conditions and data projections onto other species reveal overarching functional and evolutionary pressures impacting the translation system and bacterial fitness, underscoring the utility of systematic screens for investigating protein synthesis, adaptation, and evolution.

INTRODUCTION

Protein synthesis is a complex, essential, and adaptive process, orchestrated by ribosomes and a multitude of accessory factors that translate different mRNAs to meet changing physiological demands. The central role of protein synthesis in bacterial growth and fitness is emphasized by its high energy consumption (up to 40% of total *E. coli* energy turnover; Wilson and Nierhaus, 2007), the copiousness of its components during exponential growth (ribosomes constitute up to 50% of *E. coli* dry cell mass; Kjeldgaard and Gausing, 1974), and the fact that it is targeted by many antimicrobials (e.g., aminoglycosides and macrolides; Nikolay et al., 2016).

Yet, despite broad scientific interest spanning decades, many important knowledge gaps remain. For example, the complete set of factors needed for normal ribosome biogenesis is unknown (Kaczanowska and Rydén-Aulin, 2007). Furthermore, while ribosome assembly is closely coupled to cell growth, how these two processes are coordinated is unclear (Asato, 2005). Likewise, while translational error rates are known to vary dramatically among different physiological, mutant, and transcript sequence contexts (e.g., Poole et al., 2004), the factors governing fidelity are not fully understood.

Highly complex biological systems such as the bacterial translational machinery clearly present a great challenge to experimental biologists. To address this complexity and improve understanding, the role of individual components (genes and proteins) is established, often using cell biology, genetic, and biochemical approaches. For example, the functional relationships of the individual components to each other can be measured using a qualitative genetic screen. Here, pairs of genes are simultaneously mutationally inactivated and the net phenotypic effect (which may be neutral, greater than expected based on the single gene phenotypes, or less than expected) informs us of the functional relationship between the two genes (i.e., an epistatic/functional relationship or genetic interaction [GI]). Thus, gene pairs may show positive (i.e., alleviating or suppressive), negative (aggravating or antagonistic), or neutral (i.e., no functional overlap detected) relationships. Recent developments in large-scale GI screen technology offer the potential to produce GI maps in a system-wide manner under different environmental conditions (Bandyopadhyay et al., 2010). These datasets can substantially improve understanding of the global molecular architecture of the processes involved, and they can serve as the basis for subsequent studies, both experimental

and computational. Notably, pairwise GI data can be transformed into higher order modular maps, where the modules represent functionally coherent sets of genes, protein complexes, and/or biochemical pathways.

Decades of investigations of bacterial translation included forward genetic screens that have led to the ad hoc identification and characterization of individual *E. coli* protein synthesis genes and pairwise dependencies (e.g., new translation genes identified as suppressors of temperature-sensitive mutations in known translation factors; see Gagarinova and Emili, 2015 and references therein). However, progress in the systematic global mapping of GIs underlying bacterial protein synthesis has been limited (Gagarinova and Emili, 2015). For example, only five translation genes have been subjected to *E. coli* synthetic genetic array (eSGA) screens in a single condition, and none were assessed using analogous genetic interaction analysis technology for *E. coli* (see Babu et al., 2014, Gagarinova and Emili, 2012, and references therein). Thus, few GIs have been reported to date for the bacterial protein synthesis machinery (see Gagarinova and Emili, 2015 and references therein). Even less is known about how this connectivity is impacted by changing environmental demands.

We therefore reasoned that comprehensive quantitative GI surveys in *E. coli* would be especially informative for addressing gaps in our understanding of bacterial translation (Gagarinova and Emili, 2012, 2015). To this end, we used high-throughput eSGA technology to systematically examine GIs for translation genes and for representatives of uncharacterized genes and other functional categories in four conditions (Figures 1A and 1B). In addition to the standard eSGA condition, we investigated genetic dependencies at both low and high temperatures in rich media (Luria-Bertani [LB]) and under standard temperature in minimal media to approximate, in the laboratory, adjustments in temperature and nutrient availability seen during a normal bacterial life cycle. Briefly, we arrayed a collection of *E. coli* F^- recipient strains, each bearing a kanamycin (Kan)-marked mutation of a single gene, onto 384-colony plates. We then conjugated the array to high-frequency recombination (Hfr) *E. coli* donor strains, each with a single chloramphenicol (Cm)-marked query mutation, to generate and test all possible pairwise donor-recipient mutant gene combinations.

After chromosomal transfer and homologous recombination, viable double mutants were grown on Cm- and Kan-containing media in each of the four selected conditions (Figure 1A). After outgrowth, double-mutant fitness (i.e., growth) was determined by measuring colony sizes. GI relationships within each condition were then recorded as GI scores (or static GI scores), calculated by comparing the observed double-mutant fitness to predictions based on a model assuming null non-interaction between genes (Figure 1C). Finally, to quantitatively and statistically evaluate GI rewiring (i.e., GI change) underlying adaptation to each of the three additional selected conditions, we calculated differential GI scores (Figures 1D and 1E).

As expected, given the tight association between protein synthesis and microbial growth (Asato, 2005), GIs in all tested conditions involved a bona fide translation gene significantly more frequently than was expected by chance (i.e., translation gene GIs were overrepresented in all static networks), highlighting the centrality of protein synthesis for growth in all tested conditions. Analysis of these static GI maps revealed modularity and high connectivity between functionally related components, leading to the identification and independent verification of genes required for normal translation. These included *yhbY*, a broadly conserved gene (Barkan et al., 2007), for which we established a previously unappreciated role in 16S rRNA maturation and 30S ribosomal assembly. Our findings are especially notable in view of the lack of phenotypic effect of deleting annotated protein synthesis genes (e.g., *rlmJ*; Golovina et al., 2012).

In contrast, while GI rewiring between conditions was observed, it did not predominantly center on protein synthesis. Rather, GI patterns of translation genes (including translation initiation, elongation, and termination factors; translation regulators; and ribosomal (r-) proteins; see Table S1) changed relatively little between conditions. We also found other patterns in our GI data. For example, proteolysis genes interacted significantly less frequently than expected in all static GI networks, and localization and transport genes were enriched among all differential GI datasets.

As we further detail below, our static and differential GI networks reflected known functions and provided insights about previously underappreciated relationships. The full set of GI maps is a useful resource for guiding detailed gene function studies and for investigating the molecular underpinnings of environmental adaptation (Figure 1F). Projections of these data onto other species provide insights into the evolutionary pressures governing gene conservation and genetic exchange.

RESULTS

Comprehensive System-wide eSGA Screens

We used our robotic eSGA screening platform to generate all possible pairwise double-mutant combinations from a defined set of 312 genes (49 essential and 263 non-essential), encompassing virtually all annotated translation factors, ribosomal and ribosome biogenesis genes, in addition to select unannotated genes and representatives of other essential systems, like cell division (Table S1; Figure 1B; Supplemental Experimental Procedures). In total, we assessed functional relationships for >48,000 non-redundant gene pairs under the following four different culture conditions: on LB rich media at standard (32°C), low (16°C), and high (42°C) temperature (RM, LT, and HT, respectively), and on minimal media (MM) at 32°C (Figure 1A). To ensure data quality, we included multiple replicates and stringent controls, e.g., independent verification of double-mutant colony sizes and ensuring that selection with Cm or Kan, which target translation, did not confound the fitness of protein synthesis gene mutants (Figure S1A). The reproducibility of the double-mutant colony size measurements from independent conjugations (R = 0.8, Figure S1B) was consistent with high data quality.

GI Scoring

We evaluated six distinct GI-scoring approaches (see the Experimental Procedures, Table S2, and Figures S1D–S1G and S2). Briefly, GI scoring was optimized and benchmarked against several published datasets to describe the following: (1) the

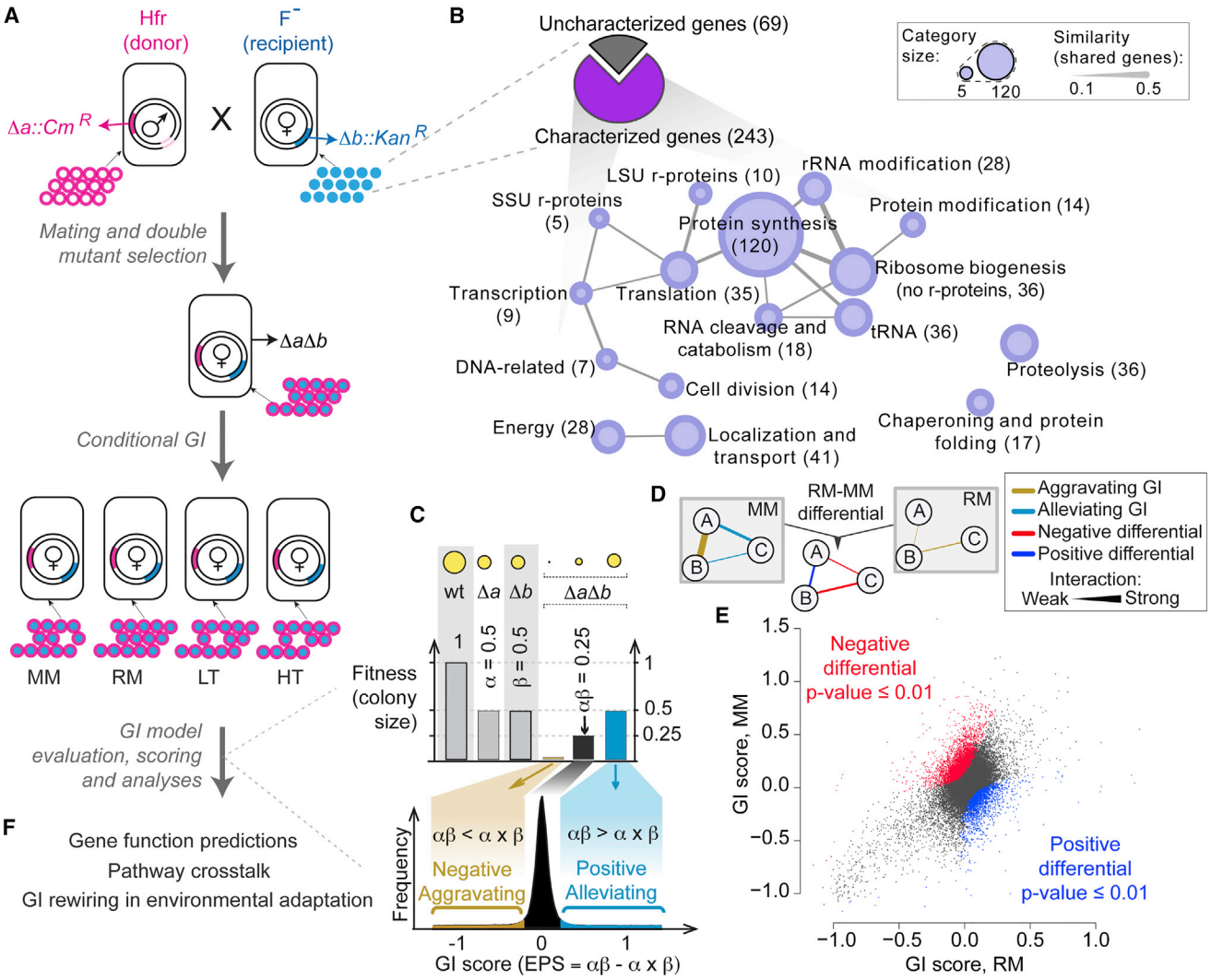

Figure 1. Mapping GI Networks Underlying Protein Synthesis in *E. coli*

(A) Schematic of eSGA screens. After bacterial conjugation (mating of single mutants) and selection, double-mutant colony sizes were monitored under RM, LT, HT, and MM culture conditions (Cm, chloramphenicol; Kan, kanamycin; ^{R}, resistance; RM, standard rich media; LT, low temperature; HT, high temperature; MM, minimal media).

(B) Screens encompassed all known and amenable to eSGA translation and ribosome biogenesis genes, representatives of other core bacterial processes, and selected unannotated genes.

(C) Multiplicative model GI scores (also referred to as static or within-condition GI scores) were calculated as the difference between the observed double-mutant colony size and the product of the corresponding individual single-mutant colony sizes (i.e., expected fitness). Significant negative or positive GI scores reflect double-mutant fitness measurements significantly worse (aggravating) or better (alleviating) than expected, respectively.

(D) RM-MM differential GIs reflect differences (or rewiring) between the RM and MM static GIs; a diagrammatic example is shown (see also E).

(E) Scatterplot comparing RM and MM static GI scores, with relationships consistent with rewiring (i.e., significant RM-MM differential GI scores) at p values $\leq$ 0.01 highlighted in red and blue. RM-LT and RM-HT differential GI scores were analogously calculated.

(F) Analyses of static and differential GI networks revealed gene function(s), pathway crosstalk, and insights about rewiring within the framework of environmental adaptation.

See also Figures S1 and S2; Tables S1, S2, S3, and S5; and the main text for references and details.

magnitude and polarity (i.e., positive or negative) of the direct GI between each gene pair, (2) the relationship between each gene pair under different environmental conditions, and (3) the similarity of GI profiles for each gene pair. This latter metric captures broadly shared functions by quantifying the extent of interaction sharing by any two genes.

According to the selected, functionally informative product (or multiplicative) model of GIs, the fitness of a strain with two functionally unrelated mutations is expected to equal the product of the fitness of the respective single mutants (Mani et al., 2008); a GI score is then calculated as the difference between the observed and expected double-mutant fitness measurements

(Figures 1C, S1D–S1G, and S2; Tables S2 and S3; Supplemental Experimental Procedures). Benchmarking revealed that this method of scoring eSGA data captures insights missed by conventional forward suppressor screens (Figure S2C; Table S2; Supplemental Experimental Procedures). Furthermore, significant product GI scores were recorded for most translation gene pairs previously reported to interact genetically (Figure S1D). Data informativeness was also evident in a complementary metric based on the overall similarity of GI patterns (i.e., GI profile Pearson correlation coefficients [GI-PCCs]; Table S4), with both GI scores and GI-PCCs reflecting functional relationships (Figure S2; Table S2).

GI Rewiring between Conditions

To statistically evaluate GI rewiring or quantitative differences between RM static GI scores and their respective counterparts in each of the other conditions (Figure S3A), we calculated differential GI scores (Bandyopadhyay et al., 2010). Thus, for example, RM-MM differential GI network reflects rewiring between RM and MM static GI networks (Figures 1D and 1E; Table S5; Supplemental Experimental Procedures). In all differential GI datasets, score directionality (i.e., positive or negative) indicates how the double-mutant GI score in RM compares to that in the second of the two conditions (Figures 1D and 1E). For instance, RM-MM significant positive differential GI indicates that the GI score for the pair of genes is significantly reduced in MM compared to RM (i.e., the double-mutant fitness is higher in RM).

As expected from differences between static GIs (Figure S3A), GI rewiring between conditions was observed (Table S5). Specifically, we detected 9,419, 5,856, and 5,892 RM-MM, RM-LT, and RM-HT differential GIs, respectively, with p values $\leq$ 0.05 (corresponding counts of extreme differential GIs with p values $\leq$ 0.001 were 1,459, 785, and 731, respectively). These numbers indicate that MM is most different from RM in terms of GIs. Clustering autocorrelations (i.e., Pearson correlation coefficients of each gene's GI profile in RM versus another condition; Table S6) indicated that MM was most different from RM in terms of GI patterns (Figures S3B and S3C).

GI rewiring is functionally informative. For example, an unannotated gene, *yjbM*, was enriched (p value 0.018) for RM-LT negative differential GI scores with cell envelope-related localization genes (Tables S1 and S5). These included *ftsY*, an inner membrane protein with pleiotropic effects on cell division (Vicente et al., 2006), suggesting a potential differential LT effect of *yjbM* deletion on cell division. Consistent with this, *ΔyjbM* mutant cell lengths were significantly different from wild-type at low, but not at standard, temperature (Figure S3D).

Protein Synthesis Is Central to Fitness but Shows Limited Rewiring in Response to Environmental Change

Translation genes were significantly overrepresented in all significant static GI datasets (Figure 2A), attesting to the translation's importance for growth in all respective conditions. Consistent with this, bona fide translation genes exhibited substantive crosstalk within conditions (Figures 2B and S3E). In contrast, translation genes were not overrepresented among differential GIs (Figure 2A). Rather, genes whose products directly participate in protein synthesis (i.e., genes in translation manually curated category, which includes translation initiation, elongation, and termination factors; translation regulators; and r-proteins as well as genes in r-protein categories; see Table S1) tended to have high autocorrelations (Figure 2C; Table S6), emphasizing the entrenched dependencies of the core translation machinery. There were also interesting patterns of GIs across functional categories in static GI datasets. For example, enrichments for alleviating interactions among translation, tRNA production, and chaperoning and protein folding categories (Figure 2D) are consistent with sub-processes interacting with each other as modules in a pathway leading to protein production, with impaired translation reducing cellular demand for charged tRNA and thereby lifting pressure on a generalist chaperoning machinery. This is also consistent with increased chaperone expression facilitating protein production in *E. coli* (e.g., Kolaj et al., 2009).

Proteolysis genes stood out in contrast to translation genes as interacting significantly less frequently than expected in all static networks, which was consistent with infrequent process-level crosstalk of proteolysis genes (Figures 2A, S3E, and S4A). Likewise, in contrast to translation, GIs underlying several categories had undergone significant rewiring (Figure 2A). For example, localization and transport genes were enriched among all differential GI datasets; RM-LT differential GIs were enriched for chaperoning and protein folding genes; and cell division differential GIs were significantly overrepresented in the RM-MM dataset (Figure 2A).

Taken together, these observations reveal pathway-level crosstalk in static GI maps and GI rewiring under different environmental conditions, while highlighting the centrality and entrenched dependencies of the core protein synthetic machinery.

GI Networks Predict Genes Vital for Normal Translation

The rich data (Table S2; Figure S2) allowed us to predict the functions of unannotated genes affecting translation in RM with high precision. We first determined GI-based associations of each gene to translation (Figures S4B and S4C) to systematically identify and focus on unannotated genes with the most prominent links to translation. Strikingly, when we ranked all genes by the total number of associations with translation (Figures S4B and S4C), several unannotated genes outranked most known translation genes (Figure 3A), pointing to possible roles in protein synthesis. From these, we sampled 12, showing a range of associations but tending toward higher association ranks, to verify roles in translation (Figure 3). First, we assessed translational fidelity in each of the corresponding single mutants in comparison to a parental wild-type strain or single mutants lacking bona fide translation genes (i.e., Δ*rlmE*, Δ*rng*, or Δ*lepA*). For this, we used reporter plasmids encoding either wild-type beta-lactamase (LacZ) or mutant variants that are non-functional unless a specific translation error occurs.

Strikingly, the deletion of each of these candidate genes resulted in impaired translational fidelity (Figure 4A) comparable to, or greater than, that observed in the absence of translational proofreading factor EF4 (LepA) (Qin et al., 2006) or Rng or RlmE, whose deletions increase or reduce error rates (Roy-Chaudhuri et al., 2010; Widerak et al., 2005), respectively. For example,

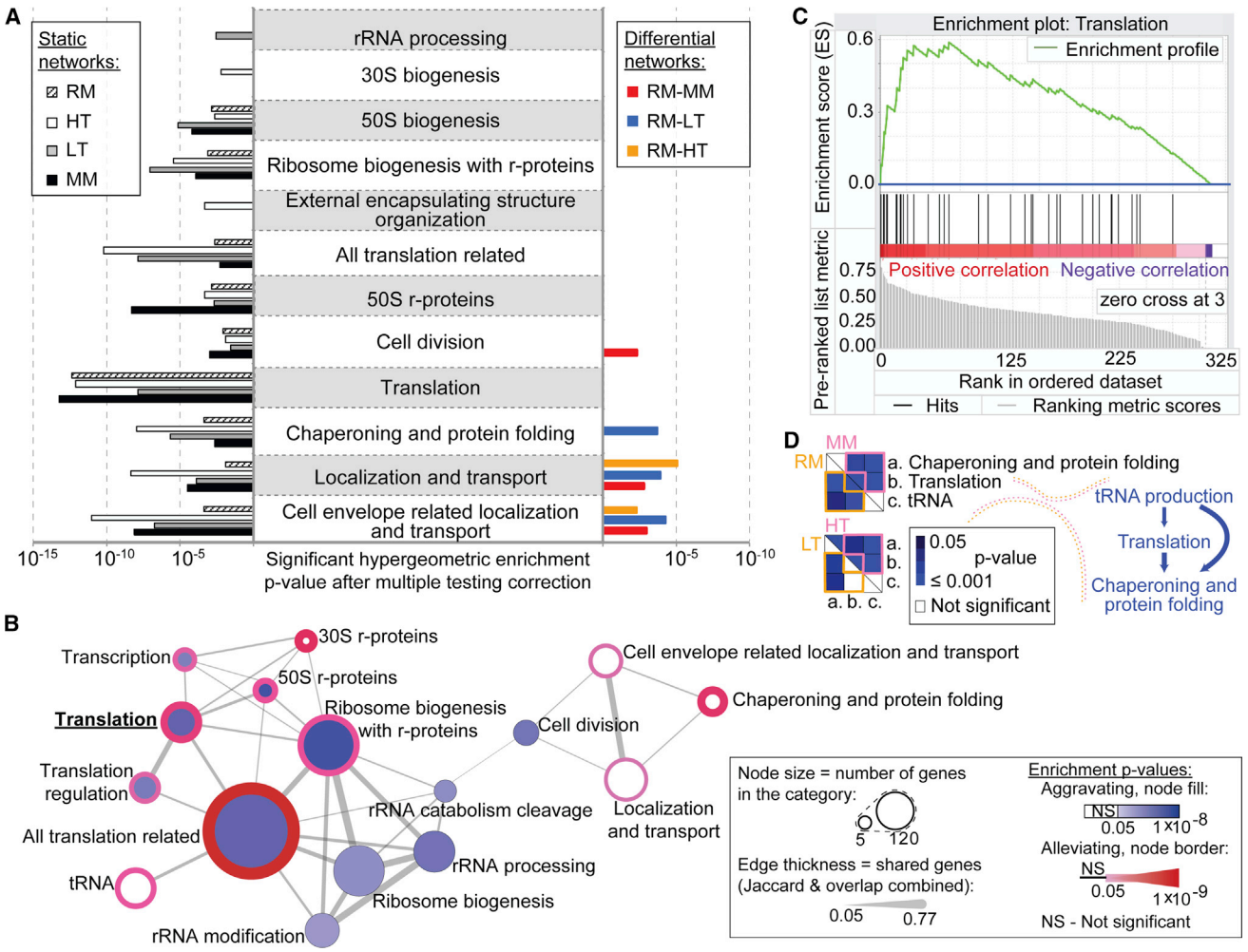

Figure 2. GI Network Connectivity and Rewiring under Different Culture Conditions

(A) Overrepresentation of select curated functional categories in the static and differential GI networks. Multiple-testing-corrected hypergeometric enrichment p values ($\leq$0.05) are shown.

(B) Schematic summarizing enrichments for RM GIs between annotated translation genes (bold, underlined) and components of other categories. Shared memberships between categories with combined similarity coefficient p values $\leq 5 \times 10^{-3}$ and false discovery rates (FDRs) ≤ 0.1 are shown as edges (Merico et al., 2010).

(C) Translation, large ribosomal subunit protein, and small ribosomal subunit protein genes tend to have high autocorrelations (Gene Set Enrichment Analysis (GSEA) nominal p values < 0.01 and FDR < 0.2). A representative RM-MM GSEA plot for translation genes is shown. Enrichment score plot (at the top) expresses a Kolmogorov-Smirnov-like statistic, reflecting the degree to which the values for the genes within the selected category (i.e., translation in this case, black vertical lines in the middle of the plot) are overrepresented at the extremes of the entire pre-ranked list (bottom).

(D) Example of process-level crosstalk across conditions. Heatmaps compare enrichments for alleviating GIs between select categories in MM versus RM and LT versus HT. Corresponding process-level pathway diagram with arrows, representing enrichments for between-process alleviating GIs, is shown at right; this is consistent with alleviating GIs, expected between members of a gene-level pathway (Gagarinova and Emili, 2012).

See also Figures S3 and S4A; Tables S1, S3, S5, and S6; and the main text for references and details.

deleting *ychP*, *yjiA*, *yhgF*, *ycbZ*, *yigZ*, *ybfN*, or *yggE* increased the rate of UGA stop codon readthrough 50- to 90-fold over baseline. Complementation plasmids, but not mock control plasmids, rescued the fidelity and fitness defects (Figures 4B and S4D–S4F), confirming that the phenotypes were target related and not due to spurious secondary mutations.

We also examined ribosomal profiles and 23S rRNA processing in the corresponding mutants (Figures 4C, 4D, and S4G). Phenotype and GI differences between these translation-associated genes (Figures 3, 4, and S4G; Tables S3, S4, S5, and S6) suggested that they are likely involved in different aspects of the translation process.

GIs Predict the Role of YhbY in 16S rRNA Processing

YhbY is a broadly conserved putative RNA-binding protein (Barkan et al., 2007). Consistent with our data (Figures 3 and 4; Table S3), *yhbY* was shown to be required for normal 23S rRNA processing and 50S biogenesis (Barkan

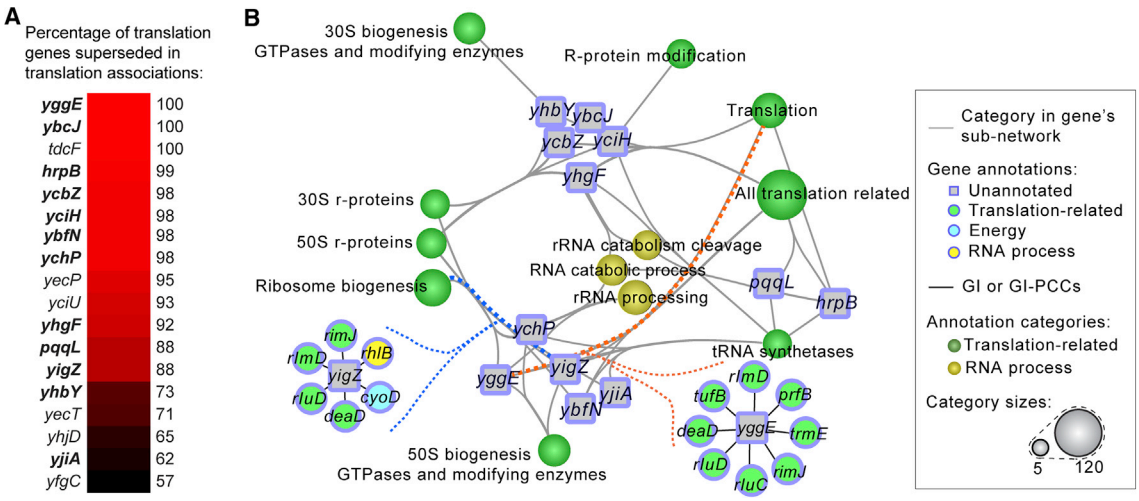

Figure 3. GIs Implicate Unannotated Genes in Protein Synthesis

(A) Certain unannotated genes supersede annotated translation genes in terms of the number of GI-derived associations to translation. Genes selected for follow-up experiments are highlighted in bold.

(B) Extensive associations of selected unannotated genes with translation-related categories, grouped according to functional similarity, with nodes (genes and categories) and edges (associations) placed to simplify the display. Examples of relationships used to derive associations to translation categories (highlighted with dashed lines) are illustrated.

See also Tables S1, S3, and S4 and Figure S4.

et al., 2007). However, our GI data also suggested links to the assembly of the 30S subunit (Figure 3; Table S3). This pointed to a potentially underappreciated impact of YhbY on ribosome biogenesis. To examine if GI links to 30S biogenesis reflected noise in the data or provided real new functional information, we chose YhbY for a closer functional examination.

The rRNA precursor transcript is cleaved by RNase III (Rnc) to release precursor 17S, 23S, and 5S rRNA and tRNA fragments (Kaczanowska and Rydén-Aulin, 2007; Figure 5A). During normal 30S subunit biogenesis, 17S rRNA precursor is then cleaved by nucleases Rne, Rng, Rnr, Rnb, Rph, and Pnp, with any one of Rph, Rnr, Rnb, and Pnp being sufficient for the 3′ end of 16S rRNA cleavage (Figure 5A; Kaczanowska and Rydén-Aulin, 2007; Sulthana and Deutscher, 2013). Cleavage and modification of rRNA and concomitant r-protein incorporation are facilitated by accessory factors (Era, RimM, RimP, RbfA, YbeY, and RsgA; Figure 5A; Davies et al., 2010; Kaczanowska and Rydén-Aulin, 2007; Nord et al., 2009). GIs of *yhbY* with a number of genes required for 30S biogenesis (Figure 5A) are consistent with YhbY's involvement in 30S biogenesis.

To examine this directly, we performed primer extension assays on wild-type and Δ*yhbY* strains, which established the preferential accumulation of incompletely processed 5′-end 16S rRNA cleavage precursor in the mutant cells (Figure 5B). Consistent with these results, we identified YhbY in the 30S as well as 50S fractions (Figure S4H).

YhbY Is Required for Proper 30S and 50S Subunit Assembly

Given that rRNA processing occurs as r-proteins are sequentially incorporated during subunit assembly (see Kaczanowska and Rydén-Aulin, 2007 and references therein), we hypothesized that *yhbY* depletion perturbs the binding of specific 30S r-proteins and biogenesis factors. Indeed, quantitative mass spectrometry revealed significantly reduced amounts (1.4-, 28-, 2-, and 2-fold, respectively) of S5, RimM, Rne, and RsmC (a 16S rRNA methyltransferase that binds the 30S subunit, but not free rRNA; Tscherne et al., 1999) in the 30S fraction in the mutant relative to wild-type, whereas S13 and RbfA were significantly increased (1.6- and 2.4-fold, respectively). These changes support our GI-based predictions, providing independent evidence for the requirement of YhbY for normal 30S biogenesis.

While YhbY previously was shown to impact 50S subunit biogenesis (Barkan et al., 2007), which 50S r-proteins are affected was not known. Our data addressed this. Notably, *yhbY* interacts genetically with genes encoding r-proteins L1, L4, L23, L32, and L35, which are added at early through late stages of 50S biogenesis (Chen and Williamson, 2013). Correspondingly, we detected changes in the abundances of various large subunit r-proteins in the mutant relative to the wild-type in 30S fraction, where early 50S subunit biogenesis intermediates were found (Figure 6). Only late-binding 50S r-proteins were affected in the 50S fraction (Figure 6). In addition, we found that the abundance of DeaD, an RNA helicase required for normal 50S biogenesis and 5′ cleavage of 23S rRNA (see Kaczanowska and Rydén-Aulin, 2007 and references therein), was reduced 2-fold in 30S and 50S fractions in the mutant relative to the wild-type. Similarly, in the 50S fraction, the abundances of the 23S rRNA pseudouridine synthases RluB and RluC (see Kaczanowska and Rydén-Aulin, 2007 and references therein) as well as Rne were reduced 2-, 2-, and 4-fold, respectively.

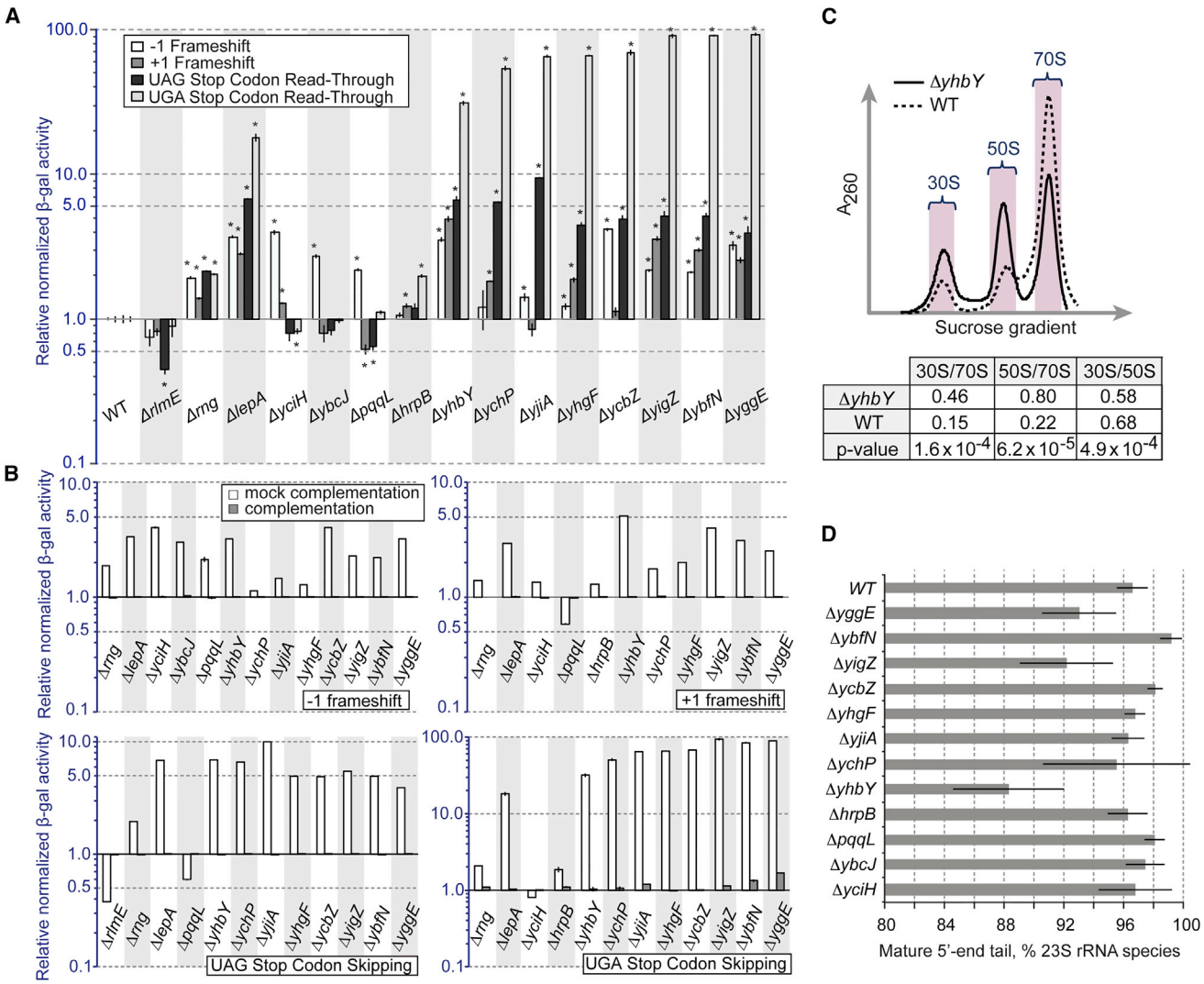

	30S/70S	50S/70S	30S/50S
ΔyhbY	0.46	0.80	0.58
WT	0.15	0.22	0.68
p-value	1.6×10^{-4}	6.2×10^{-5}	4.9×10^{-4}

Figure 4. Normal Protein Synthesis Requires Predicted Translation-Associated Unannotated Genes

(A) Translational fidelity in selected mutants, positive controls (*ΔrlmE*, *Δrng*, and *ΔlepA*), and wild-type (WT). Plot shows frameshift or stop codon skipping rates, as reflected in β-galactosidase (β-gal, functional LacZ) activity after normalizing relative to WT and correcting for differences in native (non-mutant) LacZ expression. *, significantly different mutant and WT measurements, Bonferroni multiple testing-corrected two-tailed t test, p value ≤ 0.05.

(B) Complementation, but not mock control plasmids, rescued significant mutant translational fidelity defects (from A). All measurements were normalized to the corresponding WT controls.

(C) Deletion of YhbY leads to an abnormal ribosomal profile with altered ratios of subunits and 70S ribosomes. Representative ribosomal profile plots for *ΔyhbY* and WT, mean ratios, and two-tailed t test p values are shown.

(D) Primer extension analysis of 5'-end tails of 23S rRNA in WT and selected mutant strains.

Combined measurements reflect means of at least three independent replicates; error bars represent standard deviation (SD).

See also Figures S4D and S4G.

DISCUSSION

Protein synthesis is an elaborate, conserved, and adaptive process. Forward genetic screens have led to crucial discoveries, such as the identification of ribosome biogenesis factors and translational fidelity control dependencies (e.g., see Gagarinova and Emili, 2015 and references therein). However, few GIs had been reported for the *E. coli* protein synthesis machinery. Hence, for this study, we undertook systematic large-scale screening to shed more light on the functional organization of the *E. coli* protein synthesis machinery. To facilitate follow-up investigations, all our GI data are freely available via a dedicated online portal (http://ecoli.med.utoronto.ca/eMap/PS/).

As expected, translation genes were highly connected in all static GI maps (Figures 2A, 2B, and S3E), consistent with the importance of protein synthesis for growth across conditions. The utility of these networks is highlighted by the resulting functional insights, particularly the inference of unannotated genes

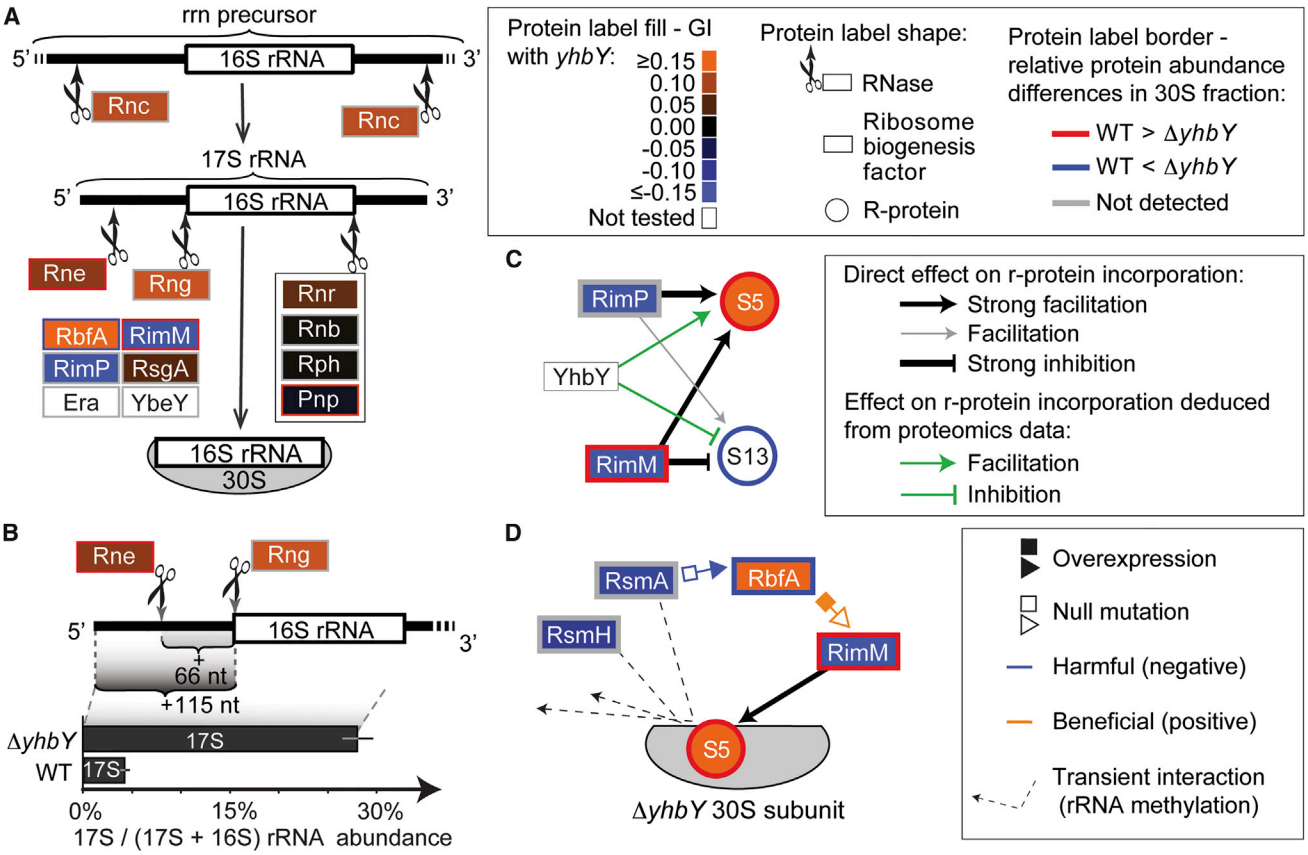

Figure 5. YhbY Is Required for 30S Biogenesis

(A) Schematic shows annotated RNases and co-factors required for efficient 16S rRNA cleavage and 30S biogenesis.

(B) Primer extension analysis showing the accumulation of 17S rRNA precursor in *ΔyhbY* cells, compared to WT (unequal variance two-tail t test p value < 0.01). Averages of three independent measurements are shown; error bars reflect SDs.

(C) GIs of *yhbY* with *rimM* or *rimP* are consistent with functional buffering with respect to influence on S13 and S5 incorporation.

(D) GI and proteomics data implicate YhbY in decoding center formation and a potential 30S biogenesis checkpoint.

See also Table S3 and the main text for references and details.

required for normal protein synthesis, which is especially significant in view of the extensive previous studies and the limited deletion phenotypes of certain annotated components (e.g., *rlmJ*; Golovina et al., 2012).

Independent evidence supports the involvement of some of the identified genes in protein synthesis. For example, YbcJ has an r-protein S4-like domain that is predicted to bind structured RNA (Volpon et al., 2003). YciH is a homolog of eukaryotic translation initiation factor 1 (eIF1) with effects on translational output in vivo and on translation initiation fidelity in vitro (see Osterman et al., 2015 and references therein), which are consistent with the mutant translational fidelity defects (Figures 4A and 4B). YigZ is a widely conserved nucleic acid-binding protein, whose closest mammalian homolog, IMPACT, is involved in translational regulation in the developing nervous system (see Roffé et al., 2013 and references therein). Overexpressing *yggE* increases *E. coli* growth rate (Kim et al., 2005), consistent with a role in a growth rate-limiting process. YjiA is a member of the ubiquitous, but largely uncharacterized, COG0523 family of putative GTPases (Sydor et al., 2013), which is notable because GTP hydrolysis is required for many steps in translation (see Kaczanowska and Rydén-Aulin, 2007 and references therein). While the diversity of these observations and corresponding mutant deletion phenotypes (Figures 3, 4, and S4G; Tables S3, S4, S5, and S6) indicate different roles, the absence of annotated homologs and high gene conservation in a number of instances suggest our findings are broadly relevant. Hence, while their exact mechanistic roles remain to be established, our GI data can motivate and help guide future follow-up investigations.

YhbY is an illustrative example. It previously was reported to be required for normal 23S rRNA maturation and 50S biogenesis (Barkan et al., 2007). Our study indicates that YhbY likely affects 50S biogenesis at an early stage. Specifically, reduced incorporation of the early-binding L22, which does not exchange between ribosomes and r-protein pools in vitro (Pulk et al., 2010), in *ΔyhbY* mutants suggests that YhbY is required for normal 50S biogenesis at or before the point of L22 incorporation (Figure 6). The alleviating GI between genes encoding YhbY and L4 (Table S3), which is incorporated

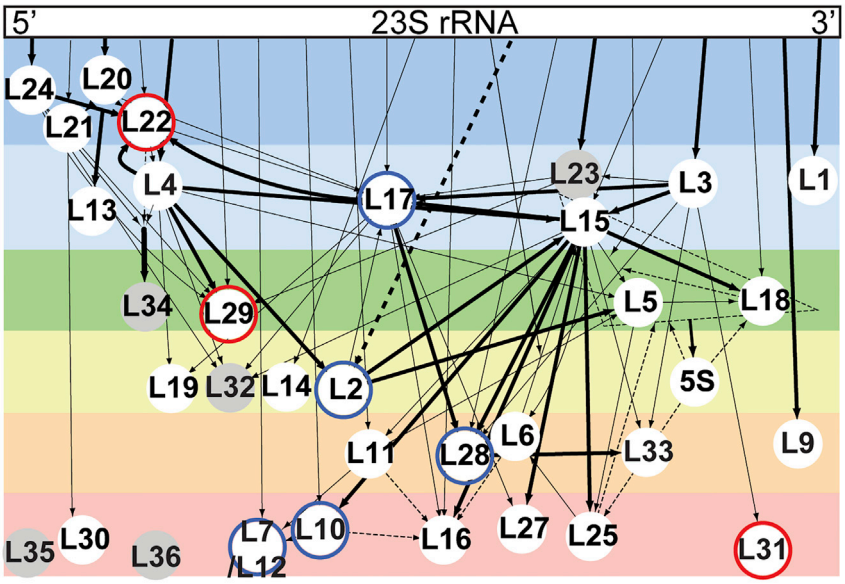

Relative r-protein abundance differences:

- WT < Δ*yhbY*
- WT > Δ*yhbY*
- Not significant (NS)
- Not identified

R-protein assembly groups:

1 early binding
2
3
4
5
6 late binding

Protein	WT/Δ*yhbY* in 30S fraction	WT/Δ*yhbY* in 50S fraction
L22	6 / 1	NS
L17	1 / 7	NS
L29	4 / 1	NS
L2	1 / 2	NS
L28	1 / 4	NS
L10	1 / 5	1 / 3
L7 / L12	1 / 4	1 / 2
L31	2 / 1	2 / 1

Figure 6. YhbY Is Required for Normal 50S r-Protein Incorporation

Schematic of large ribosomal subunit assembly, showing relative r-protein abundance differences between *ΔyhbY* and WT in the 30S fraction, where early large ribosomal subunit biogenesis intermediates are found, and in the 50S fraction, where more mature products are present (assembly groups and map based on Chen and Williamson, 2013). Relative protein abundances were measured by precision mass spectrometry; arrows within the assembly map indicate influence on binding (i.e., the binding of proteins at arrow tips depends on protein or rRNA at arrow origin, with wider lines indicating stronger effects).

cooperatively with L22 during early 50S biogenesis (see Kaczanowska and Rydén-Aulin, 2007 and references therein), highlights the importance of YhbY for this step in the assembly of the large ribosomal subunit.

The incorporation of a number of other 50S r-proteins, including L28, was affected in the absence of YhbY (Figure 6). While precursor pools tend to be larger for earlier binding r-proteins, L28, one of the later binding 50S r-proteins, is a notable exception (Chen et al., 2012; Chen and Williamson, 2013). As L28 levels in 50S biogenesis precursors increased in the absence of YhbY (Figure 6), YhbY may play a role in the correct ordering of 50S r-protein incorporation.

Our GI data also indicated a previously unknown role of YhbY in 30S biogenesis. For example, reduced abundance of S5 in *ΔyhbY* 30S fraction and the alleviating GI between *yhbY* and *rpsE* (encoding S5) are consistent with YhbY facilitating S5 incorporation (Table S3; Figure 5C). Moreover, the increased abundance of S13 and the reduced abundance of S5 in Δ*yhbY* 30S fraction and the aggravating GIs of *yhbY* with *rimM* or *rimP* are consistent with YhbY functionally buffering (1) the inhibition of S13 incorporation by RimM and (2) the facilitation of S5 incorporation by RimM or RimP, which are observed in vitro (Bunner et al., 2010) (Figure 5C). The loss of RimP results in the depletion of S5, but not S13 (Sashital et al., 2014), consistent with the GI between *yhbY* and *rimP* resulting from effects on S5 incorporation (Figure 5C).

S5 is located near the ribosome-decoding center and is important for translational fidelity (see Gagarinova and Emili, 2015 and references therein), with reduced S5 recruitment and increased error rates in Δ*yhbY* (Figures 4A, 4B, and 5C) potentially manifesting defective decoding center formation. As RsmA (KsgA) and RsmH are 16S rRNA methyltransferases, essential for normal ribosomal fidelity and acting on the 30S subunit (Desai and Rife, 2006; Kimura and Suzuki, 2010), the aggravating GIs of *yhbY* with *rsmA* and *rsmH* (Figure 5D; Table S3) may reflect negative cumulative effects of reduced fidelity or, at least in the case of RsmA, failure of one or more 30S biogenesis checkpoints. RsmA and RbfA functions are linked to segregating immature and mature initiation-competent 30S subunits (Connolly and Culver, 2013). In the presence of excess RbfA, which was observed in the *ΔyhbY* 30S fraction (Figure 5D), RsmA is required for S21 incorporation, 16S rRNA maturation, translation initiation fidelity, and overall translational capacity (Connolly and Culver, 2013). Hence, the aggravating GI between *yhbY* and *rsmA* we observed (Figure 5D) is expected and underlines the consistency between our data and the literature. Similarly, the increased abundance of ribosome-decoding site-binding RbfA, coincident with the reduction in RimM in the *ΔyhbY* 30S fraction (Figure 5D), is consistent with RbfA overexpression suppressing *rimM*$^-$ mutant fitness defects (Bylund et al., 2001). While additional experiments are warranted, the aggravating *rimM-yhbY* and the alleviating *rbfA-yhbY* GIs with coincident protein-level changes (Figure 5D) implicate YhbY in 30S biogenesis and in efficient RsmA-mediated (Connolly and Culver, 2013) ribosome biogenesis checkpoint progression.

The GI maps also reveal many other potentially relevant and interesting dependencies. For example, *rimP* is a 30S subunit

biogenesis factor whose deletion preferentially reduces fitness at high temperature (Nord et al., 2009). Five of its ten RM-HT differential GI with annotated genes were with cell division or cell envelope-related localization genes, including *secB* and a related *dnaJ* gene (see Table S5 and below). Notably, SecB overexpression suppresses the temperature sensitivity and aggregation phenotypes of a strain lacking DnaK, DnaJ, and trigger factor (Ullers et al., 2004), of which only DnaJ results in temperature sensitivity (Nichols et al., 2011). These significant differential GIs raise the hypothesis that the RimP requirement for high-temperature adaptation may be linked to the roles of these functionally related genes, particularly SecB and DnaJ.

A number of other specific hypotheses also arise from our GI networks. First, the understanding of some functional relationships, e.g., those underlying proteolysis, may require higher-order (e.g., triple) mutation combinations (Figure S4A). Second, given pronounced chaperoning and protein folding RM-LT rewiring and enrichment for aggravating GIs in LT (Figures 2A and S3E), genes with corresponding positive RM-LT differential GIs are candidates for roles in protein folding.

Third, one can speculate that significant RM-MM differential GIs (Table S5) reflect adaptation to growth on MM, including anabolic pathway activation and transition to slower growth via translation inhibition. While we did not focus on genes required for translation inhibition, e.g., during stationary phase, our study included several genes encoding translation-inhibiting factors. Specifically, RsfA (RsfS) is a ribosome-silencing factor that impairs subunit joining (Häuser et al., 2012). Strains lacking RsfA show reduced viability in stationary cultures and delayed growth after a shift from rich to poor growth medium (Häuser et al., 2012). Ribosome modulation factor (RMF) and hibernation-promoting factor (HPF) inhibit translation in stationary or slowly growing cells by making 100S ribosomal dimers (Ueta et al., 2008; Wada et al., 2000), while protein Y (pY; YfiA) inhibits translation by blocking the binding of aminoacyl-tRNA in cell-free translation systems (Agafonov et al., 2001).

While the aforementioned translation-inhibiting genes did not interact with each other genetically in RM (Table S3), significant positive RM-MM differential GI occurred between *rsfA* and *hpf* (p value 0.0019; Table S5). Furthermore, GIs of *rsfA* and *hpf* with *ftsY* were significantly rewired between RM and MM (p values 0.017 and 0.00015, respectively; Table S5), and a strong RM-alleviating GI was observed between *rsfA* and *ftsY*. Notably, depletion of FtsY was reported to lead to RMF upregulation and the inhibition of translation (Bürk et al., 2009). These data are consistent with (1) RsfA- and HPF-mediated translation inhibition pathways buffering each other during the shift to minimal media (i.e., at least one translation inhibition mechanism must be functional for normal adaptation to slower growth), and (b) one or both ribosome-silencing pathways involving a functional link to FtsY.

Significant GI rewiring between RM and MM also was recorded for *rmf-rsfA* and *pY-hpf* gene pairs (Table S5). HPF and pY were suggested to have opposite roles during 100S ribosome dimer formation, with HPF deletion mutant producing no 100S particles because pY inhibited their formation in the presence of RMF (Ueta et al., 2005). The RM-MM differential GI between *hpf* and *pY* (Table S5) reflects double-mutant fitness improvement in MM compared to RM, consistent with the loss of both genes allowing cells to adapt to slower growth by preventing complete inactivation of RMF-mediated translation inhibition (Table S5). These data point to previously underappreciated functional links among ribosome-silencing factors, and they exemplify how differential GI data can provide additional avenues for understanding gene roles and relationships.

Fourth, while translation genes were not enriched among differential GIs (Figure 2A), adaptation to changing environmental contexts involved global rewiring of GIs underlying other processes (e.g., localization and transport; Figure 2A). Therefore, the close coupling between protein synthesis and growth (Asato, 2005) may be achieved not through the dramatic rewiring of translation gene GIs as we expected, but through a combination of some GI changes and adjustments via intrinsic balancing mechanisms within the protein synthesis apparatus (Figure 2A). The existence of such balancing mechanisms is supported by a number of observations, including, for example, the synergistic or opposing roles of specific residues and components of the ribosome in translational fidelity control (e.g., see Ogle et al., 2002 and references therein). At the same time, protein synthesis apparatus has a huge capacity for adjustment, which may be utilized during environmental adaptation. For example, peptidyl transferase site reaction rates on ribosomes from *E. coli* versus *Thermus thermophilus*, whose optimal growth temperature is 35°C higher, both increase with temperature to a similar maximum rate at their respective optima (Rodriguez-Correa and Dahlberg, 2008). Nonetheless, overall protein synthesis rates under optimal culture conditions are 10–15 times slower in vivo compared to in vitro (Rodriguez-Correa and Dahlberg, 2008), which implies room for modulation. Combining multiple point mutations in essential genes and rRNA with each other and with whole or partial gene deletions may reveal the mechanisms that serve to regulate protein synthetic activities on a finer scale to map the smallest units required for performing any given function and for ensuring successful environmental adaptation.

Our results also have evolutionary implications. First, regardless of growth condition, the distributions of functionally informative GI scores were shifted toward positive (alleviating) values (Figures S1G and S2; Supplemental Experimental Procedures). Since random scores should center on zero (i.e., no interaction), a similar trend in analogous yeast SGA studies was interpreted as supporting the notion that genetic exchange (i.e., sexual reproduction) improves fitness (Mani et al., 2008). Our data, similarly, have implications for the longstanding debate over the evolution of sexual reproduction (i.e., bacterial conjugation) (de Visser and Elena, 2007; Otto, 2008), supporting an earlier conjecture (Beerenwinkel et al., 2007) with more data, conditions, and GI models. Second, our data suggest that gene essentiality and the degree and type of connectivity also must be considered when evaluating gene conservation (see the Supplemental Experimental Procedures for details). Third, our data point to questions regarding the apparent lack of conservation of GI networks across species based on comparing single static maps from each species (e.g., Roguev et al., 2008). As gene- and process-level functional dependencies can change significantly even between relatively similar conditions (e.g.,

Figures 2A and S3), the GI patterns recorded for a single condition capture only a fraction of relationships important to an organism's fitness. Hence, more meaningful cross-species comparisons would evaluate evolutionary rewiring in the context of conditional rewiring. Given the high conservation of the protein synthesis machinery (Figure S5), our GI maps represent an excellent starting point for investigating evolutionary and environmental changes in functional networks.

EXPERIMENTAL PROCEDURES

eSGA Screens and GI Scoring

Strain handling, donor construction, plate-based conjugation, double-mutant generation, and colony imaging were performed essentially as previously described (Babu et al., 2014; see the Supplemental Experimental Procedures for details and additional controls). After mating and dual drug selection, viable double mutants were replica pinned in 1,536-colony format and grown in the following four conditions: standard/RM (LB, 32°C), LT (16°C, LB), HT (42°C, LB), and MM (32°C, M9 minimal media). After standard plate imaging, colony size measurement, and normalization, we calculated additive, multiplicative, minimum fitness, log, log2, and E-score GI scores (see the Supplemental Experimental Procedures for details). GI-PCCs were calculated after removing 30 kb linkage (Figure S1C). Probability values for GIs and GI-PCCs, after filtering for 30 kb linkage and self-correlations, respectively, were determined using a distribution-based approach (Babu et al., 2014). GI scores and GI-PCCs were benchmarked by comparing the distributions for functionally associated versus randomly drawn gene pairs using the Kolmogorov-Smirnov non-parametric test as described previously (Babu et al., 2011) (see Table S2 and the Supplemental Experimental Procedures for details). Differential GIs and p values (Table S5) were calculated as described previously (Bandyopadhyay et al., 2010). Autocorrelations (Table S6) were calculated by correlating each gene's GI pattern in RM with the same gene's GI profile from each of the other conditions after removing a 30-kb linkage suppression window.

Gene Functional Category Associations

Unless otherwise indicated, manually curated annotations were used for analyses and are referred to in the paper (Supplemental Experimental Procedures; Table S1). Gene functional category associations were determined by partitioning GI and GI-PCC RM networks and assigning functions to uncharacterized genes based on the functions of annotated genes within their corresponding sub-networks (see Figures S4B and S4C and the Supplemental Experimental Procedures). For this, first, we created three datasets from probability-filtered (p value $\leq$ 0.05) GI scores as follows: (1) positive, (2) negative, and (3) union of positive and negative. Similarly, three GI-PCC datasets were created for a total of six GI and GI-PCC datasets. Subsequently, each dataset was partitioned into local sub-networks by either applying the Markov clustering algorithm as described previously (see Hu et al., 2009 and references therein) or by isolating the first neighbor network of each gene.

The lists of genes within each resulting sub-network were tested for overrepresentation of manually curated functional categories using the hypergeometric enrichment analysis via the Bingo Cytoscape plug-in (Maere et al., 2005). Gene functional category associations for unannotated genes were established as follows: if an uncharacterized gene was part of a Markov cluster containing a greater than expected number of genes belonging to a particular category, it was assigned the corresponding association; similarly, if a gene's first neighbor network was enriched for a given category, an association between the gene and that function was made.

Associations to all translation categories, across network-partitioning methods and datasets, were summed up for each gene. Genes were then ranked by total number of associations (high to low); unannotated genes with one or more associations to a translation category (Benjamini-Hochberg multiple testing corrected p value $\leq$ 0.05; Benjamini and Hochberg, 1995) were included in Figure 3A. Gene functional category associations were similarly determined for cell division in RM and LT to assess conditional roles, with *yjbM* being selected for follow-up as a result.

Phenotypic Assays and Other Analyses

BW25113 (parental Keio deletion/recipient strain, see Babu et al., 2014 and references therein) was used as wild-type control in follow-up experiments alongside select single-gene deletion mutants. Unless otherwise indicated, RM growth condition was used. Primer extension (Nord et al., 2009); cell staining, imaging, and length measurement (Babu et al., 2011); northern blot hybridizations (Charollais et al., 2003); and translational fidelity assays (O'Connor et al., 1992) were performed essentially as described previously, at least in triplicate (see the Supplemental Experimental Procedures for details).

Ribosomal subunits and ribosomes were separated by gradient sedimentation (see the Supplemental Experimental Procedures for details). Protein compositions of 30S and 50S peaks from Δ*yhbY* and wild-type logarithmic cultures (optical density 600 [OD_{600}] of 0.3–0.4) were compared by combining ^{18}O-based stable isotope labeling with quantitative tandem mass spectrometry analyses (White et al., 2009). A 95% confidence cutoff was applied to identifications. Distribution models and 95% fold change confidence intervals for each fraction and protein set (i.e., 30S or 50S biogenesis) were individually determined from respective 1:1 (w:w) WT:WT and mutant:mutant mixtures. Relative differences between WT and mutant, exceeding the corresponding 95% fold change confidence interval, were considered significant (p value $\leq$ 0.05; see the Supplemental Experimental Procedures for details).

Hypergeometric analyses with Benjamini-Hochberg multiple testing correction were used to test for GI enrichment and underrepresentation in static and differential networks after filtering GI data for significance (p values $\leq$ 0.05 and $\leq$ 0.01, respectively) (see the Supplemental Experimental Procedures for details). Long-term evolutionary conservation of each *E. coli* gene was expressed as counts of species with orthologs detected by InParanoid (Ostlund et al., 2010). Pre-ranked Gene Set Enrichment Analysis (GSEA) was performed using a desktop application (Subramanian et al., 2005).

SUPPLEMENTAL INFORMATION

Supplemental Information includes Supplemental Experimental Procedures, five figures, and six tables and can be found with this article online at http://dx.doi.org/10.1016/j.celrep.2016.09.040.

AUTHOR CONTRIBUTIONS

A. Gagarinova and A.E. conceived the project. Experiments were performed by A. Gagarinova, G.S., B.S., H.A., V.D., C.A.W., N.B., and A.F.Y. Data were analyzed by A. Gagarinova, S.P., and C.A.W. The paper was drafted by A. Gagarinova and A.E., with input from G.S., B.S., C.A.W., A. Golshani, M.B., and E.D.B.

ACKNOWLEDGMENTS

The authors acknowledge constructive discussions with members of the A.E., E.D.B., and M.B. laboratories; technical support from Oxana Pogoutse; and helpful advice from J.J. Diaz-Mejia, J. Vlasblom, and R. Arnold (University of Toronto). We thank J. Greenblatt, J. Parkinson, and J. Brumell (University of Toronto) for insightful suggestions; H. Mori (Keio University) for providing recipient strains; and M. O'Connor (University of Missouri-Kansas City) for providing plasmid p90.91. The authors thank G. Cagney (University College Dublin) for editing advice. This work was supported by grants to A.E. (Canadian Institutes of Health Research [CIHR] MOP-82852), E.D.B. (Canada Research Chair in Microbial Chemical Biology, CIHR Foundation grant 143215, Natural Sciences and Engineering Research Council of Canada [NSERC] Discovery grant), and NSERC grants to A. Golshani and M.B. (DG-20234). A. Gagarinova was a recipient of Vanier Canada and Ontario Graduate Scholarships.

Received: September 24, 2014
Revised: July 30, 2016
Accepted: September 14, 2016
Published: October 11, 2016

REFERENCES

Agafonov, D.E., Kolb, V.A., and Spirin, A.S. (2001). Ribosome-associated protein that inhibits translation at the aminoacyl-tRNA binding stage. EMBO Rep. *2*, 399–402.

Asato, Y. (2005). Control of ribosome synthesis during the cell division cycles of E. coli and Synechococcus. Curr. Issues Mol. Biol. *7*, 109–117.

Babu, M., Díaz-Mejía, J.J., Vlasblom, J., Gagarinova, A., Phanse, S., Graham, C., Yousif, F., Ding, H., Xiong, X., Nazarians-Armavil, A., et al. (2011). Genetic interaction maps in Escherichia coli reveal functional crosstalk among cell envelope biogenesis pathways. PLoS Genet. *7*, e1002377.

Babu, M., Arnold, R., Bundalovic-Torma, C., Gagarinova, A., Wong, K.S., Kumar, A., Stewart, G., Samanfar, B., Aoki, H., Wagih, O., et al. (2014). Quantitative genome-wide genetic interaction screens reveal global epistatic relationships of protein complexes in Escherichia coli. PLoS Genet. *10*, e1004120.

Bandyopadhyay, S., Mehta, M., Kuo, D., Sung, M.K., Chuang, R., Jaehnig, E.J., Bodenmiller, B., Licon, K., Copeland, W., Shales, M., et al. (2010). Rewiring of genetic networks in response to DNA damage. Science *330*, 1385–1389.

Barkan, A., Klipcan, L., Ostersetzer, O., Kawamura, T., Asakura, Y., and Watkins, K.P. (2007). The CRM domain: an RNA binding module derived from an ancient ribosome-associated protein. RNA *13*, 55–64.

Beerenwinkel, N., Pachter, L., Sturmfels, B., Elena, S.F., and Lenski, R.E. (2007). Analysis of epistatic interactions and fitness landscapes using a new geometric approach. BMC Evol. Biol. *7*, 60.

Benjamini, Y., and Hochberg, Y. (1995). Controlling the false discovery rate: a practical and powerful approach to multiple testing. J. R. Stat. Soc. Series B Stat. Methodol. *57*, 289–300.

Bunner, A.E., Nord, S., Wikström, P.M., and Williamson, J.R. (2010). The effect of ribosome assembly cofactors on in vitro 30S subunit reconstitution. J. Mol. Biol. *398*, 1–7.

Bürk, J., Weiche, B., Wenk, M., Boy, D., Nestel, S., Heimrich, B., and Koch, H.G. (2009). Depletion of the signal recognition particle receptor inactivates ribosomes in Escherichia coli. J. Bacteriol. *191*, 7017–7026.

Bylund, G.O., Lövgren, J.M., and Wikström, P.M. (2001). Characterization of mutations in the metY-nusA-infB operon that suppress the slow growth of a DeltarimM mutant. J. Bacteriol. *183*, 6095–6106.

Charollais, J., Pflieger, D., Vinh, J., Dreyfus, M., and Iost, I. (2003). The DEAD-box RNA helicase SrmB is involved in the assembly of 50S ribosomal subunits in Escherichia coli. Mol. Microbiol. *48*, 1253–1265.

Chen, S.S., and Williamson, J.R. (2013). Characterization of the ribosome biogenesis landscape in E. coli using quantitative mass spectrometry. J. Mol. Biol. *425*, 767–779.

Chen, S.S., Sperling, E., Silverman, J.M., Davis, J.H., and Williamson, J.R. (2012). Measuring the dynamics of E. coli ribosome biogenesis using pulse-labeling and quantitative mass spectrometry. Mol. Biosyst. *8*, 3325–3334.

Connolly, K., and Culver, G. (2013). Overexpression of RbfA in the absence of the KsgA checkpoint results in impaired translation initiation. Mol. Microbiol. *87*, 968–981.

Davies, B.W., Köhrer, C., Jacob, A.I., Simmons, L.A., Zhu, J., Aleman, L.M., Rajbhandary, U.L., and Walker, G.C. (2010). Role of Escherichia coli YbeY, a highly conserved protein, in rRNA processing. Mol. Microbiol. *78*, 506–518.

de Visser, J.A., and Elena, S.F. (2007). The evolution of sex: empirical insights into the roles of epistasis and drift. Nat. Rev. Genet. *8*, 139–149.

Desai, P.M., and Rife, J.P. (2006). The adenosine dimethyltransferase KsgA recognizes a specific conformational state of the 30S ribosomal subunit. Arch. Biochem. Biophys. *449*, 57–63.

Gagarinova, A., and Emili, A. (2012). Genome-scale genetic manipulation methods for exploring bacterial molecular biology. Mol. Biosyst. *8*, 1626–1638.

Gagarinova, A., and Emili, A. (2015). Investigating bacterial protein synthesis using systems biology approaches. Adv. Exp. Med. Biol. *883*, 21–40.

Golovina, A.Y., Dzama, M.M., Osterman, I.A., Sergiev, P.V., Serebryakova, M.V., Bogdanov, A.A., and Dontsova, O.A. (2012). The last rRNA methyltransferase of E. coli revealed: the yhiR gene encodes adenine-N6 methyltransferase specific for modification of A2030 of 23S ribosomal RNA. RNA *18*, 1725–1734.

Häuser, R., Pech, M., Kijek, J., Yamamoto, H., Titz, B., Naeve, F., Tovchigrechko, A., Yamamoto, K., Szaflarski, W., Takeuchi, N., et al. (2012). RsfA (YbeB) proteins are conserved ribosomal silencing factors. PLoS Genet. *8*, e1002815.

Hu, P., Janga, S.C., Babu, M., Díaz-Mejía, J.J., Butland, G., Yang, W., Pogoutse, O., Guo, X., Phanse, S., Wong, P., et al. (2009). Global functional atlas of Escherichia coli encompassing previously uncharacterized proteins. PLoS Biol. *7*, e96.

Kaczanowska, M., and Rydén-Aulin, M. (2007). Ribosome biogenesis and the translation process in Escherichia coli. Microbiol. Mol. Biol. Rev. *71*, 477–494.

Kim, S.Y., Nishioka, M., Hayashi, S., Honda, H., Kobayashi, T., and Taya, M. (2005). The gene yggE functions in restoring physiological defects of Escherichia coli cultivated under oxidative stress conditions. Appl. Environ. Microbiol. *71*, 2762–2765.

Kimura, S., and Suzuki, T. (2010). Fine-tuning of the ribosomal decoding center by conserved methyl-modifications in the Escherichia coli 16S rRNA. Nucleic Acids Res. *38*, 1341–1352.

Kjeldgaard, N.O., and Gausing, K. (1974). Regulation of biosynthesis of ribosomes. In Ribosomes, P. Lengyel, M. Nomura, and A. Tissières, eds. (Cold Spring Harbor, New York: Cold Spring Harbor Laboratory), pp. 369–392.

Kolaj, O., Spada, S., Robin, S., and Wall, J.G. (2009). Use of folding modulators to improve heterologous protein production in Escherichia coli. Microb. Cell Fact. *8*, 9.

Maere, S., Heymans, K., and Kuiper, M. (2005). BiNGO: a Cytoscape plugin to assess overrepresentation of gene ontology categories in biological networks. Bioinformatics *21*, 3448–3449.

Mani, R., St Onge, R.P., Hartman, J.L., 4th, Giaever, G., and Roth, F.P. (2008). Defining genetic interaction. Proc. Natl. Acad. Sci. USA *105*, 3461–3466.

Merico, D., Isserlin, R., Stueker, O., Emili, A., and Bader, G.D. (2010). Enrichment map: a network-based method for gene-set enrichment visualization and interpretation. PLoS ONE *5*, e13984.

Nichols, R.J., Sen, S., Choo, Y.J., Beltrao, P., Zietek, M., Chaba, R., Lee, S., Kazmierczak, K.M., Lee, K.J., Wong, A., et al. (2011). Phenotypic landscape of a bacterial cell. Cell *144*, 143–156.

Nikolay, R., Schmidt, S., Schlömer, R., Deuerling, E., and Nierhaus, K.H. (2016). Ribosome assembly as antimicrobial target. Antibiotics (Basel) *5*, E18.

Nord, S., Bylund, G.O., Lövgren, J.M., and Wikström, P.M. (2009). The RimP protein is important for maturation of the 30S ribosomal subunit. J. Mol. Biol. *386*, 742–753.

O'Connor, M., Göringer, H.U., and Dahlberg, A.E. (1992). A ribosomal ambiguity mutation in the 530 loop of E. coli 16S rRNA. Nucleic Acids Res. *20*, 4221–4227.

Ogle, J.M., Murphy, F.V., Tarry, M.J., and Ramakrishnan, V. (2002). Selection of tRNA by the ribosome requires a transition from an open to a closed form. Cell *111*, 721–732.

Osterman, I.A., Evfratov, S.A., Dzama, M.M., Pletnev, P.I., Kovalchuk, S.I., Butenko, I.O., Pobeguts, O.V., Golovina, A.Y., Govorun, V.M., Bogdanov, A.A., et al. (2015). A bacterial homolog YciH of eukaryotic translation initiation factor eIF1 regulates stress-related gene expression and is unlikely to be involved in translation initiation fidelity. RNA Biol. *12*, 966–971.

Ostlund, G., Schmitt, T., Forslund, K., Köstler, T., Messina, D.N., Roopra, S., Frings, O., and Sonnhammer, E.L. (2010). InParanoid 7: new algorithms and tools for eukaryotic orthology analysis. Nucleic Acids Res. *38*, D196–D203.

Otto, S.P. (2008). Sexual reproduction and the evolution of sex. Nature Education *1*, 182.

Poole, E.S., Major, L.L., Cridge, A.G., and Tate, W.P. (2004). The mechanism of recoding in pro- and eukaryotes. In Protein Synthesis and Ribosome Structure (Wiley-VCH Verlag GmbH), pp. 397–428.

Pulk, A., Liiv, A., Peil, L., Maiväli, U., Nierhaus, K., and Remme, J. (2010). Ribosome reactivation by replacement of damaged proteins. Mol. Microbiol. *75*, 801–814.

Qin, Y., Polacek, N., Vesper, O., Staub, E., Einfeldt, E., Wilson, D.N., and Nierhaus, K.H. (2006). The highly conserved LepA is a ribosomal elongation factor that back-translocates the ribosome. Cell *127*, 721–733.

Rodriguez-Correa, D., and Dahlberg, A.E. (2008). Kinetic and thermodynamic studies of peptidyltransferase in ribosomes from the extreme thermophile Thermus thermophilus. RNA *14*, 2314–2318.

Roffé, M., Hajj, G.N., Azevedo, H.F., Alves, V.S., and Castilho, B.A. (2013). IMPACT is a developmentally regulated protein in neurons that opposes the eukaryotic initiation factor 2α kinase GCN2 in the modulation of neurite outgrowth. J. Biol. Chem. *288*, 10860–10869.

Roguev, A., Bandyopadhyay, S., Zofall, M., Zhang, K., Fischer, T., Collins, S.R., Qu, H., Shales, M., Park, H.O., Hayles, J., et al. (2008). Conservation and rewiring of functional modules revealed by an epistasis map in fission yeast. Science *322*, 405–410.

Roy-Chaudhuri, B., Kirthi, N., and Culver, G.M. (2010). Appropriate maturation and folding of 16S rRNA during 30S subunit biogenesis are critical for translational fidelity. Proc. Natl. Acad. Sci. USA *107*, 4567–4572.

Sashital, D.G., Greeman, C.A., Lyumkis, D., Potter, C.S., Carragher, B., and Williamson, J.R. (2014). A combined quantitative mass spectrometry and electron microscopy analysis of ribosomal 30S subunit assembly in E. coli. eLife *3*, e04491.

Subramanian, A., Tamayo, P., Mootha, V.K., Mukherjee, S., Ebert, B.L., Gillette, M.A., Paulovich, A., Pomeroy, S.L., Golub, T.R., Lander, E.S., and Mesirov, J.P. (2005). Gene set enrichment analysis: a knowledge-based approach for interpreting genome-wide expression profiles. Proc. Natl. Acad. Sci. USA *102*, 15545–15550.

Sulthana, S., and Deutscher, M.P. (2013). Multiple exoribonucleases catalyze maturation of the 3′ terminus of 16S ribosomal RNA (rRNA). J. Biol. Chem. *288*, 12574–12579.

Sydor, A.M., Jost, M., Ryan, K.S., Turo, K.E., Douglas, C.D., Drennan, C.L., and Zamble, D.B. (2013). Metal binding properties of Escherichia coli YjiA, a member of the metal homeostasis-associated COG0523 family of GTPases. Biochemistry *52*, 1788–1801.

Tscherne, J.S., Nurse, K., Popienick, P., and Ofengand, J. (1999). Purification, cloning, and characterization of the 16 S RNA m2G1207 methyltransferase from Escherichia coli. J. Biol. Chem. *274*, 924–929.

Ueta, M., Yoshida, H., Wada, C., Baba, T., Mori, H., and Wada, A. (2005). Ribosome binding proteins YhbH and YfiA have opposite functions during 100S formation in the stationary phase of Escherichia coli. Genes Cells *10*, 1103–1112.

Ueta, M., Ohniwa, R.L., Yoshida, H., Maki, Y., Wada, C., and Wada, A. (2008). Role of HPF (hibernation promoting factor) in translational activity in Escherichia coli. J. Biochem. *143*, 425–433.

Ullers, R.S., Luirink, J., Harms, N., Schwager, F., Georgopoulos, C., and Genevaux, P. (2004). SecB is a bona fide generalized chaperone in Escherichia coli. Proc. Natl. Acad. Sci. USA *101*, 7583–7588.

Vicente, M., Rico, A.I., Martínez-Arteaga, R., and Mingorance, J. (2006). Septum enlightenment: assembly of bacterial division proteins. J. Bacteriol. *188*, 19–27.

Volpon, L., Lievre, C., Osborne, M.J., Gandhi, S., Iannuzzi, P., Larocque, R., Cygler, M., Gehring, K., and Ekiel, I. (2003). The solution structure of YbcJ from Escherichia coli reveals a recently discovered alphaL motif involved in RNA binding. J. Bacteriol. *185*, 4204–4210.

Wada, A., Mikkola, R., Kurland, C.G., and Ishihama, A. (2000). Growth phase-coupled changes of the ribosome profile in natural isolates and laboratory strains of Escherichia coli. J. Bacteriol. *182*, 2893–2899.

White, C.A., Oey, N., and Emili, A. (2009). Global quantitative proteomic profiling through 18O-labeling in combination with MS/MS spectra analysis. J. Proteome Res. *8*, 3653–3665.

Widerak, M., Kern, R., Malki, A., and Richarme, G. (2005). U2552 methylation at the ribosomal A-site is a negative modulator of translational accuracy. Gene *347*, 109–114.

Wilson, D.N., and Nierhaus, K.H. (2007). The weird and wonderful world of bacterial ribosome regulation. Crit. Rev. Biochem. Mol. Biol. *42*, 187–219.